Acta Polytechnica **59**(3):238–247, 2019
doi:10.14311/AP.2019.59.0238

available online at http://ojs.cvut.cz/ojs/index.php/ap

NON-DESTRUCTIVE INSPECTION BY INFRARED THERMOGRAPHY OF RESISTANCE SPOT WELDS USED IN AUTOMOTIVE INDUSTRY

Lucie Forejtová[a,c,*], Tomáš Zavadil[b,c], Ladislav Kolařík[a], Marie Kolaříková[a], Jan Sova[d], Petr Vávra[d]

[a] *Czech Technical University in Prague, Faculty of Mechanical Engineering, Technická 4, 166 07 Prague, Czech Republic*

[b] *Czech Technical University in Prague, Faculty of Nuclear Sciences and Physical Engineering, Břehová 7, 115 19 Prague, Czech Republic*

[c] *ATG s.r.o., Toužimská 771, 199 00 Prague, Czech Republic*

[d] *WORKSWELL, Libocká 653/51b, 161 00 Prague, Czech Republic*

[*] corresponding author: Lucie.Forejtova@fs.cvut.cz

Abstract. Resistance spot welding (RSW) is one of the main joining technologies of thin sheets in the automotive industry. Key factors affecting the strength of the RSW joint are the nugget diameter, asymmetry, expulsions, intended surfaces, and the presence of cracks. Despite its broad use, the RSW joint quality verification is limited only to destructive testing and a limited number of non-destructive testing (NDT) methods. Most of the testing is done destructively by sampling, which assesses only systematic defects. Ultrasonic Testing (UT) is the most used NDT method to detect non-systematic defects in the RSW joints, however the probability of the defect detection of conventional testing techniques is not fully satisfactory. Other approaches were invented to deal with this situation. The article uses the currently most used NDT approach of the UT testing as a benchmark to evaluate the ability of thermographic testing to detect defective welds of the resistance spot welding in an on-line mode. The article demonstrates that the infrared thermography may find systematic process errors that are not detectable by other NDT methods by an analysis of different temperature drops measured after a constant delay time caused by different cooling dynamics of satisfactory and non-satisfactory weld joints.

Keywords: Automotive, resistance spot welding, thermography, ultrasonic testing, probability of detection.

1. Introduction

The resistance spot welding (RSW) is the most widely used method for joining thin deep-drawing steel plates in the automotive industry because it allows a unitary quality output and a high volume of production. The RSW is a welding method of mechanical joining of materials using heat and pressure causing a fusion on the contact area of the two plates between the electrode tips by resistivity Joule heat generated by the passage of the welding current through the joined materials [1, 2]. The joined plates are coated to provide a better protection for forming and corrosion protection [1].

There are many factors affecting the weld joint quality. These include, in particular, an insufficient electrode contact, defective function of welding source, improper setting of main welding parameters, and various metal quality and purity factors as the quality of electrodes, and quality of the sheets‘ surface. For this reason, it is necessary to test the spot welds to assess the information about the weld quality and to have a feedback on the welding process [3].

Spot welds are usually tested by destructive testing methods, such as chisel, shear, metallography, hardness testing, etc. However, these methods can only detect the systematic defects. The detection of non-systematic defects is mediated by non-destructive methods, including, visual (VT) and ultrasonic (UT) methods. Nevertheless, both methods can provide only a limited feedback on an incorrect set-up of the welding process [4].

The goal of this article is to verify the ability of the thermographic testing (IRT) to detect defective welds of resistance spot welding (RSW) in an on-line mode (i.e. during the welding process or immediately after the welding). It proposes to analyse a single thermograph rather than monitoring the cooling dynamics in order to save time, and therefore significantly speed-up the testing process and make it easier for an automation. For this purpose, 27 sets of samples (5 samples in one set) were used, with specifically selected main welding parameters (I, P, t). The selection was done to simulate situations with correctly selected parameters as well as parameters above the standard range acc. to ISO 14373: 2015 [5]. Samples

were compared with VT, UT, and metallography to verify the functionality of the system.

1.1. Overview of NDT methods and techniques currently used for RSW

The RSW process is used for joining of lap joints of sheets or plates. The main quality parameter is the weld nugget. The weld nugget is created on the contact area of the two welded sheets and inaccessible to outer environment. Such arrangement disallows the use of the majority of conventional NDT methods commonly used in the industry, i.e. ET (eddy current testing), MT (magnetic particle testing), PT (penetrant testing) and requires a utilization of other complicated (RT (radiographic testing), UT, VT). For that reason, the destructive testing plays significant role in the quality assurance process of the RSW method.

The standard methods used for the defect detection in resistance spot welds are the ultrasonic testing (UT) and visual testing (VT). As the visual testing can access only outer surface, it accesses the nugget only indirectly, i.e. by observing and measuring the electrode indentation of the electrode on the surface. This method can still provide a feedback on the quality of the nugget by observing expulsions [6] and provided there is a relation between the diameter, depth and ovality of the electrode indentation to the nugget size [5]

The ultrasonic testing is able to investigate the internal structure of the weld. It uses conventional UT instruments and either a wide variety of delay lines or captive water column transducers with a frequency range between 10 and 20 MHz for this purpose. Delay line transducers use a small plastic waveguide to couple the sound energy from the transducer element to the test piece. This approach uses A-scan with pulse-echo technique generating multiple back-wall echoes for the inspection. An analysis of the echo patterns (echoes' position, decay rate, etc.) provides the information about the presence of defects, insufficient nugget size as well as about significant changes in the microstructure [7, 8]. The sensitivity of the technique is, however, not considered as ideal, and therefore alternative approaches have been investigated for years. For example, the Scanmaster company attempted to use a modern UT technique of Phased Array to detect defected spot welds with additional results compared to the conventional UT, namely the nugget diameter and nugget total area [9]. Lee et al. [4] patented a scanning acoustic microscopy using an artificial neural network (ANN) model to evaluate the quality of spot welds [10]. Such application would, however, involve a significant upfront investment cost that might diminish the industrial practicality.

The Infrared Thermography is a quite new NDT method in the field of testing the resistance spot welds. In the past, various laboratories attempted to use this method with mixed results. For example, Sangyun Lee et al. [11] used the IRT for measuring the size of the nugget. Schlichting et al. [12] used the flash thermography to investigate the two typical error classes: stick welds and welds at the splash limit. Runnemalm et al. [13] derived their approach from Schlichting´s work. Both of these applications focus only on some types of defects, and therefore need to be used in a combination with the UT. Traub [14] even patented the contact thermography measurement in USA in 1980. This technique measured the temperature produced on welding tips to estimate and/or indirectly control the weld joint quality. Nevertheless, it doesn't inspect the weld itself.

Other NDT methods were also used in laboratories (e.g. electromagnetic, micromagnetic, 3MA [8]), but they didn't reach industrial-level use so far.

Above-mentioned techniques are generally labour-intensive, requiring a qualified personnel to inspect all welds and interpret the results. Considering the volume of welds to be tested in the automotive industry (above 4000 welds per car bodywork [15]), this significantly increases the variable costs of the inspection. A technique that would provide a fully automated inspection and evaluation, even on nominal basis (defect is present in the weld joint or not) would significantly reduce costs, requiring the personnel to inspect the defective welds only by conventional methods to assess defect's acceptability, rather than searching for defects.

1.2. Infrared thermography

The infrared thermography deals with a non-contact measurement and analysis of the temperature field of tested surfaces. The principle of the measurement is to capture the thermal energy radiated by the surface of the object under the investigation in the infrared spectrum of the electromagnetic radiation and to convert it into an electrical signal. Based on the amount of energy captured and its time dependency, the surface and the time distribution of the temperature field on the thermograph can be displayed, which carries information about the energy of the object (temperature) as well as about the surface properties influencing the IR radiation [16, 17].

The advantage of the non-contact thermographic measurement is to observe and display the overall temperature field of the object, which enables to observe fast temperature changes at very high temperatures.

The main source of uncertainty in determining the temperature using a thermography are the radiation processes and their parameters that affect the radiation flux from the measured object to the camera detectors. The parameter indicating the amount of the radiated energy from the surface of the object being measured is the emissivity ε [-]. The transmission parameter τ [-] of the radiation that passes from the object to the detectors (atmosphere) reduces the amount of the measured energy. External radiation sources as ambient objects and environment between the object and the camera may distort the measured

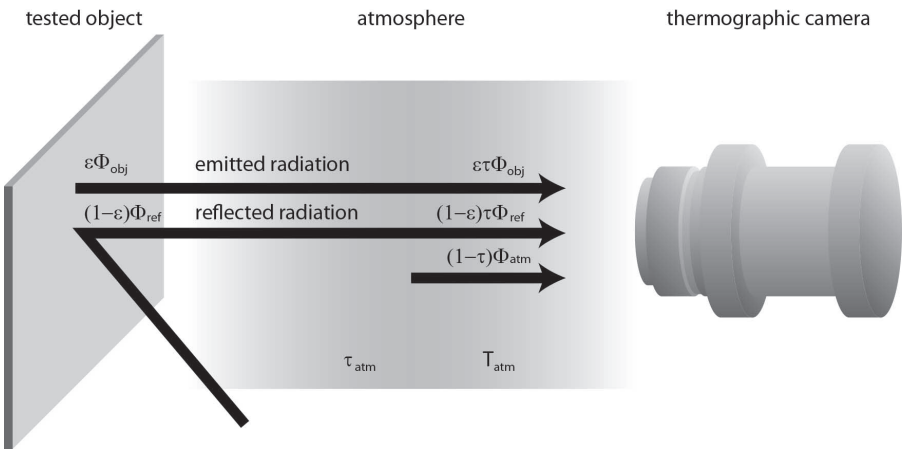

Figure 1. Principle of collecting radiation by thermographic camera.

data and make them difficult to evaluate – see Figure 1 [18, 19].

The individual components of the radiation flux received by the thermocouple detector are:

- radiation flux from the object weakened by the passage through the atmosphere: $\varepsilon\tau\phi_{obj}$,
- reflected radiation flux from surrounding sources: $(1-\varepsilon)\tau\phi_{ref}$, where $(1-\varepsilon)$ represents its reflectivity,
- radiation flux emitted by the atmosphere: $(1-\tau)\phi_{atm}$, where $(1-\tau)$ represents its emissivity.

If a full transparency of the optics of the thermographic camera optics is assumed as fully transparent and optical component's flux negligible, it is possible to compile the equation for the total radiation flux that falls on the thermographic camera's detector. This equation is sometimes referred to as the "thermography equation":

$$\phi = \sum_i \phi_i = \varepsilon\tau\phi_{obj} + (1-\varepsilon)\tau\phi_{ref} + (1-\tau)\phi_{atm} \quad (1)$$

Using the Stefann-Bolzmann law for the grey object, it would be possible to derive the relationship by which the thermographic camera calculates the temperature of the individual parts of the measured surface based on the sensor signals of the matrix detector.

The user of the thermographic camera shall set these parameters: emissivity of the object ε, phantom temperature T_{ref}, the atmospheric temperature T_{atm} and transmission of the atmosphere τ (the relative humidity and distance of the observed object to the thermographic camera is often used instead of the transmission factor).

If the surface has a low emissivity and the temperature is not significantly higher than the temperature of the environment, the reflected radiation may predominate over the original radiation significantly. That is the reason why surfaces with a high reflectivity (i.e. low emissivity) cannot be tested by thermography. Most of the welding procedures have a more favourable condition - due to the high surface temperature predominates the first part of the equation.

The correct setting of the emissivity was verified by a K-type thermocouple and a measuring unit Ahlborn Almemo 5690. The measurement spot was selected close to the weld joint (3 mm off the weld joint). The thermocouple was attached on this spot during the welding process. The measured emissivity reached $\varepsilon = 0.20$.

Due to the thermocouple usage, the real temperature of the object's temperature close to the weld joint is known. The special SW Core player from Workswell Ltd. Calculated the resulting emissivity so the observed values of the temperature would be in an accordance with the measured temperature.

1.3. Induced heat and temperature

The RSW is a welding method of mechanical joining of materials using heat and pressure causing a fusion on the contact area of the two plates between the electrode tips by resistivity Joule heat generated by the passage of the welding current through the joined materials. The spot weld is created when the current flows through the parent metal sheets that are pressed together by electrode tips. Electrical resistance on the place of the connection of the welded materials melts the sheets' material creating a metallurgical joint. The heat is, in this welding method, created directly inside the welded material, it is not introduced from the outside. A specific electrode force applied for a specific time interval is necessary for the creation of a quality weld joint.

Total induced heat Q [J] increases with the increasing electric current I [A], electric resistance R [Ω] and with the duration of the time interval t [s]. This behaviour is known as the Joule-Lenz law:

$$Q = U \cdot I \cdot t = R \cdot I^2 \cdot t \quad (2)$$

The induced heat is not constant in the whole weld area, but concentrated in the area of the highest resistance. There are several partial electrical resistances affecting the total resistance R. The current flow shall overcome the resistance of the electrodes R_e, transition resistance R_t between the electrodes and the

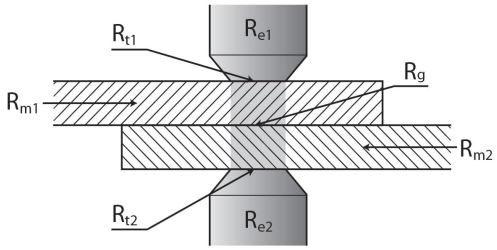

FIGURE 2. Distribution of the partial resistances of the RSW joint [7].

sheet and the resistance of the material R_m that is dependent on the cross-section of the current flow A, path length l and the specific resistance of the material ρ [Ω·m], besides the transition resistance R_g of the gap between the joined materials. The resulting total resistance is therefore:

$$R = R_{e1} + R_{e2} + R_{m1} + R_{m2} + R_{t1} + R_{t2} + R_g \quad (3)$$

The highest induced heat is generally created by the partial resistance R_g, that is, therefore, responsible for the creation of the weld joint. The undesirable heat created by electrode resistances R_e and transition resistances R_t are affected by the material of the electrodes, electrode force in the contact area and cleanliness of the contact area surfaces. A minimization of the transition resistance R_t is essential to avoid damaging the sheet surface by e.g. burning. The surface of electrodes and the welded materials, therefore, shall be perfectly clean. Material resistances R_m are provided by physical and mechanical properties of the welded materials, the path length l, weld design, and the cross-section of the current flow A, and are therefore assumed as input conditions that need to be taken into account only during the design of the welding procedure. The welding procedure is, therefore, also affected by properties of welded materials, especially material type, thickness, anticorrosion coating and number of sheets in the weld [7].

1.4. Resistance spot welding of galvanized sheet metals

The automotive industry, in order to ensure a corrosion protection, often uses galvanized sheet metals. However, galvanization adversely affects the spot welding process. As explained by Matoušek [7], the galvanization reduces the initial resistance and for this reason, the temperature curve has a less steep slope than on non-galvanized sheets. That may cause the necessity to increase the welding current or time to ensure good melting of the metal. Using higher current is, however limited from the top by creation of the weld spatter. High current results in higher temperature that causes the electrode (typically created from Cu alloys) to soften. That results in a smaller diameter of nuggets, in some cases even cold shuts. Moreover, softened Cu causes gluing of the newly used electrodes and their faster wear.

I_s [kA]	P [kN]	t_s [ms]
6	1.9	160
7	2.0	180
8	2.1	200

TABLE 1. Main welding parameters used for the experiment [20].

A perfect spot weld requires a uniform current flow though the electrodes. Uniformity can be affected also by relatively low melting temperature of the zinc coating of the welded sheets that melts at the temperature of 420 °C. During the heating process, the zinc coating is melted first, alloying the Cu electrodes. Such alloying is not uniform and it is more prominent in the centre of the electrode. This changes the transition resistance R_t, that results in a fluctuating current flow, irregular and/or small diameter nuggets.

2. Material and methods

The high-strength, deep-drawn steel DC06 (EN 10152), galvanized by zinc Zn, with a total thickness $t = 0.7$ mm and coating thickness of 4.5 μm was used. The sheets for the experiment were provided by SKODA Auto. This steel is used, for example, for the model Škoda Octavia.

Totally 135 samples (27 batches by 5 samples) with dimensions $175 \times 45 \times 0.7$ mm were welded by resistance spot welding on Dalex PMS 11-4 high-frequency welding device. The diameter of the electrodes of 4 mm is recommended for these joints by ČSN EN ISO 14373 [5]. The selected diameter of 5 mm reflects the common practice in the automotive industry. The welding current was adjusted to this change by reducing the values (effect of the electric current on the nugget size was discussed by Kolarikova et al. [21].

The samples were welded in batches. The settings verification and device maintenance was in the time gap among batches. The welding parameters were selected from the range of values as follows: welding current I of 6, 7 or 8 kA (welding current of 8 kA is being considered as exceeding the values for the common practice in the automotive industry based on the diameters used), welding time t of 160, 180 and 200 ms, and electrode force P of 1.9, 2.0, and 2.1 kN. Welding parameters were selected to create both satisfactory as well as unsatisfactory weld joints.

The welding was monitored by the FLIR A615 thermographic camera from the distance of 600 mm, top view, under 45°angle (direct angle was inaccessible due to the presence of the welding electrodes). Collected thermographs were evaluated by SW Core Player from Workswell s.r.o. (as a part of bachelor thesis of Mach [20]). The reflected radiation flux was filtered out by the software. The measured temperatures from thermographs were transformed to histograms showing the distribution for nominal temperature ranges. Median $q(T)_{1/2}$ a 95-th percentile

C [%]	Mn [%]	P [%]	S [%]	Si [%]	Ti [%]	R_e [MPa]	R_m [MPa]	A_{80} [%]
0.02	0.25	0.02	0.02	0.02	0.3	max 180	270 – 350	41

Table 2. Chemical and mechanical properties of DC06 steel.

$q(T)_{95/100}$ was determined from the histogram. The 95-th percentile worked as a low-pass filter for outlier values most likely created by the camera noise). It was expected that the unsatisfactory weld will show a median and/or 95-th percentile shift due to the change of the induced heat (e.g. caused by excessive transition resistance R_t). This approach was selected instead of the continuous monitoring of cooling dynamics in a continuous camera record mode because: 1) recording significantly prolongs the inspection time 2) metric evaluation of results is significantly more complicated 3) evaluation provides more options for subjectivity errors. The expected behaviour being verified in this experiment was that the cooling dynamics of satisfactory and non-satisfactory welds will cause the median and maximum (represented by the 95-th percentile) of the temperature drop to different nominal values after a constant delay time. Due to the steep slope of the cooling curve of the metal immediately after welding, 1 second delay was assumed satisfactory.

The VT of the weld joints was performed after the welding followed by the UT for a detection of internal defects and structural changes. Olympus Epoch 650 with V2450 delay line / water column Spot-Weld Transducer with a nominal frequency of 20 MHz and a nominal diameter of 5 mm were used for UT. The results of the UT are taken from Holub [22]. The metallographic testing was applied after the NDT testing methods to verify the size of the weld nugget, occurrence of defects and abnormalities in the heat-affected zone.

3. Results

For the purpose of this article 5 batches were selected from the total 27 batches. Batches V8, V9 and V14 satisfied the requirements for welding parameters setup and batches V19 a V20 didn't ($I = 8\,\mathrm{kA}$).

Batch V8 was welded with $I = 6\,\mathrm{kA}$, $t = 200\,\mathrm{ms}$, and $P = 2.0\,\mathrm{kN}$. The echograms of the samples demonstrated a linearily decreasing trend with a satisfactory amount of backwall echoes. The histogram of the batch V8 had the median of temperature $q(T)^{V8}_{1/2} = (36.1 \pm 0)\,^{\circ}\mathrm{C}$ and 95-th percentile $q(T)^{V8}_{95/100} = (49.38 \pm 0.76)\,^{\circ}\mathrm{C}$. The diameter of the weld was determined from the metallographic analysis as $d_n = 5.26\,\mathrm{mm}$, diameter of the HAZ as $d_{HAZ} = 6.17\,\mathrm{mm}$ (HAZ was in average 0.455 mm wide) and the depth of compression as $e_u = 0.41\,\mathrm{mm}$.

Batch V9 was welded with $I = 6\,\mathrm{kA}$, $t = 200\,\mathrm{ms}$, and $P = 2.1\,\mathrm{kN}$. The echogram of the sample V9-2 shown an unsatisfactory amount of backwall echoes with values above 20% FSH, other echograms were in norm. Subsequent tests revealed Cu from the elctrode on the surface. Histogram of the batch V9 had the median of temperature $q(T)^{V9}_{1/2} = (29.74 \pm 0.97)\,^{\circ}\mathrm{C}$ and 95-th percentile $q(T)^{V9}_{95/100} = (39.50 \pm 2.64)\,^{\circ}\mathrm{C}$. The diameter of the weld was determined from the metallographic analysis as $d_n = 4.84\,\mathrm{mm}$, diameter of HAZ as $d_{HAZ} = 6.10\,\mathrm{mm}$ (HAZ was in average 0.63 mm wide) and the depth of compression as $e_u = 0.38\,\mathrm{mm}$.

Batch V14 was welded with $I = 7\,\mathrm{kA}$, $t = 180\,\mathrm{ms}$, $P = 2.0\,\mathrm{kN}$. The echograms of the samples demonstrated a linearily decreasing trend with a satisfactory amount of backwall echoes. The histogram of the batch V14 had the median of temperature $q(T)^{V14}_{1/2} = (37.56 \pm 1.38)\,^{\circ}\mathrm{C}$ and 95-th percentile $q(T)^{V14}_{95/100} = (51.89 \pm 1.89)\,^{\circ}\mathrm{C}$. The diameter of the weld was determined from the metallographic analysis as $d_n = 5.53\,\mathrm{mm}$, diameter of HAZ as $d_{HAZ} = 6.14\,\mathrm{mm}$ (HAZ was in average 0.305 mm wide) and the depth of compression as $e_u = 0.32\,\mathrm{mm}$.

Batch V19 was welded with $I = 8\,\mathrm{kA}$, $t = 160\,\mathrm{ms}$, $P = 1.9\,\mathrm{kN}$. The echograms of the samples demonstrated a linearily decreasing trend with only 3 recognizeable backwall echoes. The weld was evaluated as burnt [22]. The histogram of the batch V19 had the median of temperature $q(T)^{V19}_{1/2} = (31.72 \pm 1.38)\,^{\circ}\mathrm{C}$ and 95-th percentile $q(T)^{V19}_{95/100} = (42.86 \pm 1.40)\,^{\circ}\mathrm{C}$. The diameter of the weld was determined from the metallographic analysis as $d_n = 5.68\,\mathrm{mm}$, diameter of HAZ as $d_{HAZ} = 6.63\,\mathrm{mm}$ (HAZ was in average 0.475 mm wide) and the depth of compression as $e_u = 0.44\,\mathrm{mm}$.

Batch V20 was welded with $I = 8\,\mathrm{kA}$, $t = 160\,\mathrm{ms}$, $P = 2.0\,\mathrm{kN}$. The echograms of the samples demonstrated a linearily decreasing trend with only 3 recognizeable backwall echoes. The weld was evaluated as burnt [22]. The histogram of the batch V20 had the median of temperature $q(T)^{V20}_{1/2} = (30.93 \pm 0.95)\,^{\circ}\mathrm{C}$ and 95-th percentile $q(T)^{V20}_{95/100} = (42.1 \pm 2.21)\,^{\circ}\mathrm{C}$. The diameter of the weld was determined from the metallographic analysis as $d_n = 4.73\,\mathrm{mm}$, diameter of HAZ as $d_{HAZ} = 5.38\,\mathrm{mm}$ (HAZ was in average 0.325 mm wide) and the depth of compression as $e_u = 0.14\,\mathrm{mm}$.

Samples V9 and V20 has the nugget diameter below the diameter of the electrode – the nugget was undersized. Sample V9 had a significantly increased size of the HAZ, probably caused by a glued electrode. Sample V20 had shallow indentation suggesting an incorrect handling during the welding procedure.

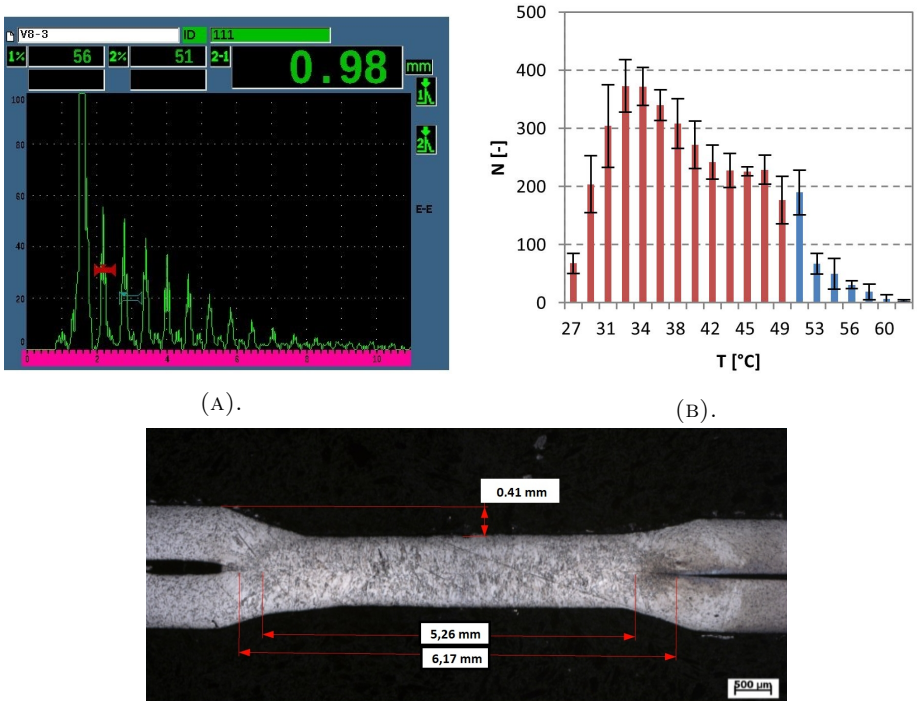

(A). (B).

(C).

FIGURE 3. Batch V8 – Echogram of the sample V8-3 by ultrasonic testing (a), histogram of measured temperatures from batch V8 by infrared thermography (b) and metallographic image of the sample V8-3 (c). Red bars indicate reach of 95-th percentile.

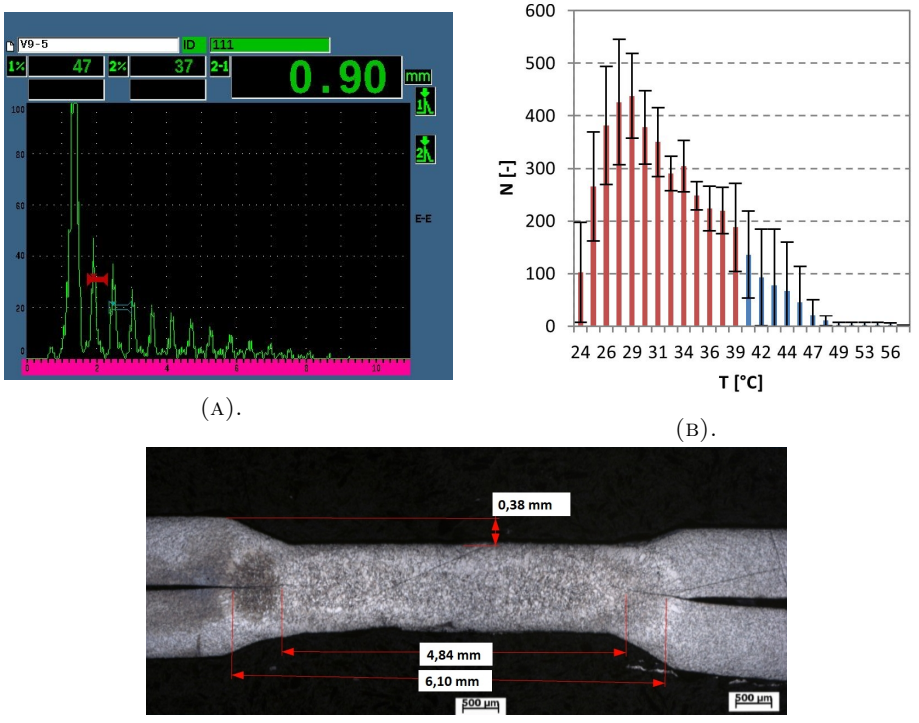

(A). (B).

(C).

FIGURE 4. Batch V9 - Echogram of the sample V9-2 by ultrasonic testing (a), histogram of measured temperatures from batch V9 by infrared thermography (b) and metallographic image of the sample V9-2 (c). Red bars indicate reach of 95-th percentile.

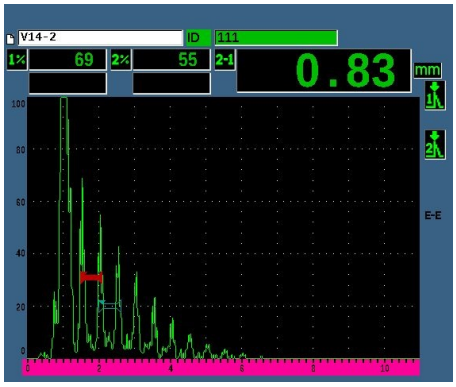

(A).

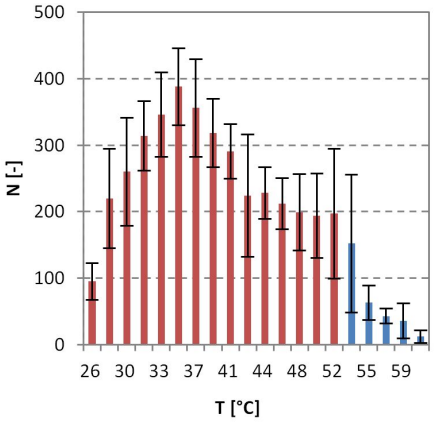

(B).

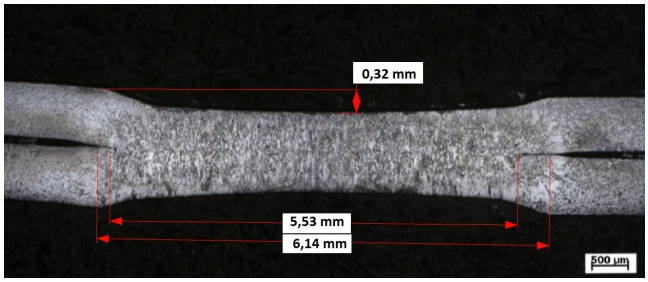

(C).

Figure 5. Batch V14 - Echogram of the sample V14-2 by ultrasonic testing (a),histogram of measured temperatures from batch V14 by infrared thermography (b) and metallographic image of the sample V14-2 (c). Red bars indicate reach of 95-th percentile.

(A).

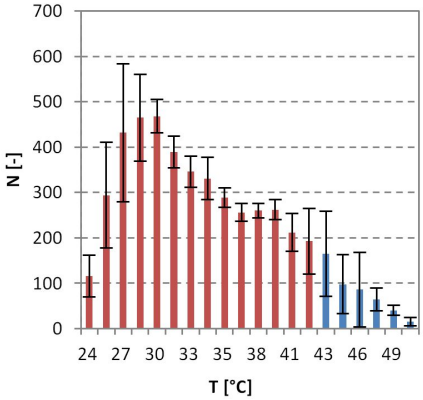

(B).

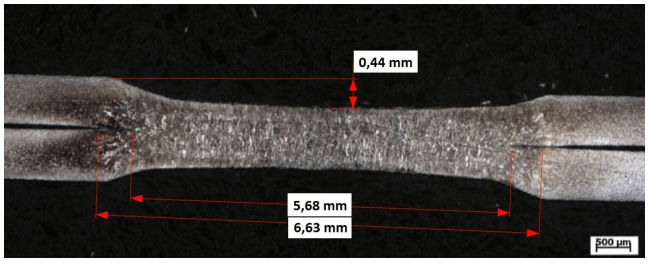

(C).

Figure 6. Batch V19 - Echogram of the sample V19-2 by ultrasonic testing (a), histogram of measured temperatures from batch V19 by infrared thermography (b) and metallographic image of the sample V19-2 (c). Red bars indicate reach of 95-th percentile.

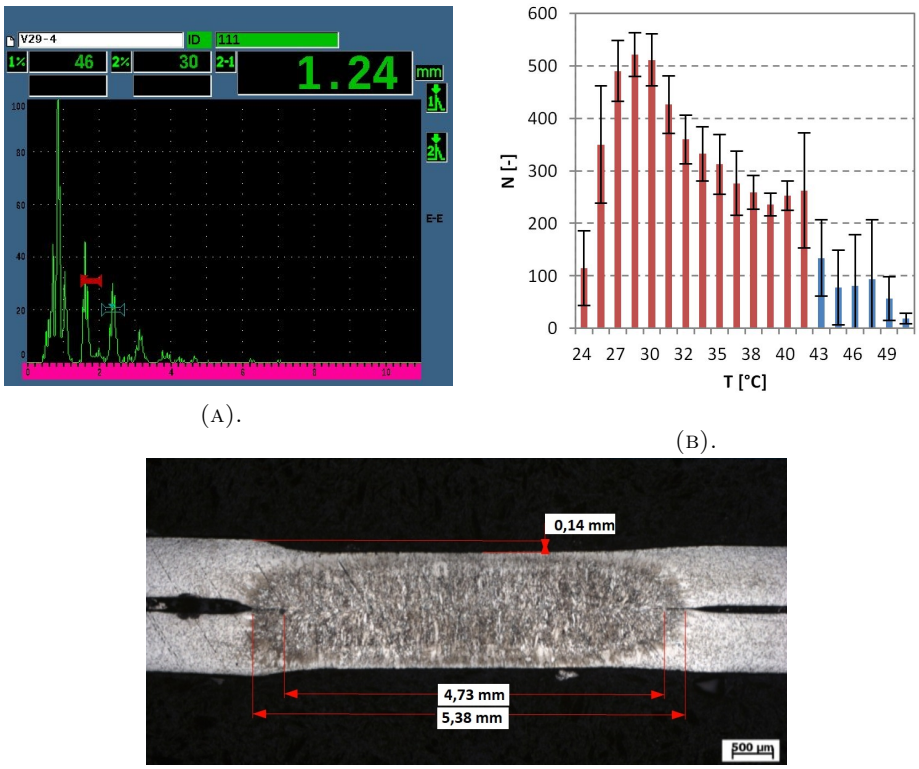

(A). (B).

(C).

FIGURE 7. Sample V20 - Echogram of the sample V20-4 by ultrasonic testing (a), histogram of measured temperatures from batch V20 by infrared thermography (b) and metallographic image of the sample V20-4 (c). Red bars indicate reach of 95-th percentile.

Sample group	#	I [kA]	t [ms]	P [kN]	d_n [mm]	w_{HAZ} [mm]	e_u [mm]	$q_{1/2}$ [°C]	$q_{95/100}$ [°C]	UT [Y/N]	IRT [Y/N]
V8	3	6	200	2	5.26	0.445	0.41	36.1	49.38	5Y	5Y
V9	2	6	200	2.1	4.84	0.63	0.38	29.74	39.5	4Y1N	1Y4N
V14	2	7	180	2	5.53	0.305	0.32	37.56	51.98	5Y	5Y
V19	2	8	160	1.9	5.68	0.475	0.44	31.72	42.86	5N	5N
V20	4	8	160	2	4.73	0.325	0.14	30.93	42.1	5N	5N

TABLE 3. Summary of the measurement results on samples V8, V9, V14, V19 and V20.

4. DISCUSSION

The batches in the experiment were selected to simulate satisfactory (V8, V9, V14) and unsatisfactory (V19, V20) requirements of ČSN EN ISO 14373 [5]. It was assumed that provided the welding procedure is obeyed and the UT and VT do not find any non-systematic defects, the results of batches V8, V9 and V14 shall satisfy the quality criteria. A correctly executed IRT in such case should have, for those batches, shown the same median and/or 95-th percentile of the temperature histogram measured by IRT.

It was observed from the results that the "unsatisfactory" batches of V19 and V20 reached an average median $\overline{q}(T)^{NA}_{1/2} \sim 31.32\,°C$ and 95-th percentile $\overline{q}(T)^{NA}_{95/100} \sim 42.48\,°C$ (see Fig. 6 and Fig. 7), which is much less than for the "satisfactory" batches V8 and V14 with average values of $\overline{q}(T)^{A}_{1/2} \sim 36.63\,°C$, resp. $\overline{q}(T)^{A}_{95/100} \sim 50.68\,°C$ (Fig. 3 and Fig. 5). The differences in median and/or 95-th percentile values is considered as the measurement uncertainty - the standard deviation σ of each of the batches never exceeded $\sigma^{max}_{q(T)1/2} = 1.38\,°C$ for median values and $\sigma^{max}_{q(T)95/100} = 2.64\,°C$ for 95-th percentile. The differences of the average values between "satisfactory" and "unsatisfactory" batches exceeded $3\sigma^{max}$ (i.e. $\overline{q}(T)^{A}_{1/2} - \overline{q}(T)^{NA}_{1/2} > 3\sigma^{max}_{q(T)1/2}$, resp. $\overline{q}(T)^{A}_{95/100} - \overline{q}(T)^{NA}_{95/100} > 3\sigma^{max}_{q(T)95/100}$).

Batch V9 satisfied the requirements of the ČSN EN ISO 14373 standard [5], however, the IRT measurement found median of $q(T)^{V9}_{1/2} = (29.74 \pm 0.97)\,°C$ and 95-th percentile of $q(T)^{V9}_{95/100} = (39.50 \pm 2.64)\,°C$ - values that fall within the range of the "unsatisfactory" group as shown on Fig. 4. A further testing by the VT and UT revealed a presence of Cu on the sheet

surface of the sample V9-2, causing the gluing of the electrode to the tested sheet. As these electrodes were maintained once the whole batch was welded, this affected the results of the rest 3 samples of the batch V9.

For isotropic material, thermal conductivity stays approximately constant and the same in all directions. However, in the case of the heavy cold pressed metals (e.g. cold-formed steels used in automotive industry) the behaviour is anisotropic and the thermal conductivity varies with the direction. Simultaneously, materials that undergone phase transformations may change their thermal conductivity abruptly [23]. It is well-known that a poorly executed welding process, especially due to high voltage, may adversely affect the microstructure by a creation of brittle phases. In the case of the RSW, this may lead to burnt welds. In burnt welds, the anisotropy of material properties as well as phases shall be changed, which affects the thermal conductivity and consequently the heat dissipation. It is, therefore, assumed that the change in heat dissipation caused the drop of the recorded median and 95-th percentile of the temperature on IRT camera.

Nominally low temperatures were a combined effect of low emissivity $\varepsilon = 0.20$ [16], longer distance from the weld of 600 mm and the angle of observation of 45°[19] due to which the absorption effect of atmosphere was magnified (see equation (1)). As the effect of atmosphere is assumed to be equally proportional to distance, lower absolute numbers are not limiting the final results.

As explained by Matoušek [7], cleanliness, flatness, and diameter of the electrode tip all play a significant role in the creation of quality RSW welds. The wear of the electrodes increases the transition resistance R_t, causing a creation of systematic defects by excessive heat on the electrodes and resulting in a reduction of the transition resistance R_g that is being responsible for the production of high-quality (satisfactory) weld, as proven in the case of batch V9. It is necessary to mention that the UT and VT methods detected only one unsatisfactory result on the sample V9-2 from the whole batch V9. That concludes that the utilization of the IRT method, in theory, may help with a detection of wear and/or damage of electrodes causing systematic errors in the welding process that cannot be easily detected by other NDT methods.

This IRT technique is able to find the presence of defects, but not their type or location in the weld joint. To assess such information, other NDT methods like UT still need to be used. Despite the fact that the UT may be robotized, the evaluation of defects needs to be done by a qualified personnel. The main potential of the IRT technique is dependent on the technique reliability. If proven reliable with selecting of defective welds, the main potential will be in a fully automated online inspection during the welding process without a necessity to inspect every weld by the NDT personnel. Information on presence of defects immediately after welding process may reduce a necessary additional time for an inspection by the UT. Instead of testing all weld joints by the UT (about 4000 weld joints are located on a car bodywork [15]), the UT testing may be then required only for those joints suspected to be defective. This may significantly shorten the average lead time and labour costs and still maintain the same level of weld quality assurance. For weld joints suspected to be defective, other NDT methods (e.g. UT) shall be used to provide information on the type of the defect, location, size and after comparison with the acceptance criteria information about the defect's acceptability.

The current research of the authors is focused on a confirmation of abovementioned claims on different types of materials, sheet thicknesses and changing environment temperature. Another important topic being investigated is the measurement uncertainty analysis depending on the equipment used, which may have a significant impact on the upfront investment costs. These research results are expected to be a part of a dissertation thesis of the main author. The utilization of the IRT as a replacement of the UT for testing of 100 % welds is currently only a potential future option to be further investigated.

5. Conclusion

The goal of this article was to verify the ability of a thermographic NDT method to detect low-quality resistance spot welds. 27 batches per 5 samples were welded by the RSW with main welding parameters selected acc. to ČSN EN ISO 14373:2015 and a common practice in the automotive industry. One part of the samples was designed to satisfy the requirements and another one to do not satisfy them. The samples were tested with one second delay after the welding by conventional a thermographic camera and the results were compared with conventional NDT methods for spot welds, e.g. ultrasonic and visual testing.

The results demonstrated that, from the histogram of measured temperatures by the thermographic camera, it is possible to group the tested samples based on the temperature median and 95-th percentile for the given time delay. The quality welds demonstrated 18 % higher temperature values than those with the low quality (evaluated as unsatisfactory for various reasons). The reason is assumed to be the altered cooling dynamics due to non-equivalent change of material properties between welds with the satisfactory or non-satisfactory quality.

This approach managed to detect a partial melting of electrodes tips and its effect on a one batch of samples. This result was observed on samples that were designed to satisfy the requirements of the standards. Other NDT methods revealed this situation only on one of the samples (due to the gluing of the electrode) and thus incorrectly interpreted the situation as a non-systematic defect.

If verified, the technique used in this article may be used for a welding procedure control to prevent a wrong setup or its non-compliance or damage or wear of the welding equipment during the welding.

The future potential of the IRT technique is given by the reliability to assess the weld condition. If proven reliable, it may provide an automated online inspection tool during the welding process that will significantly reduce the share of the UT inspections requiring an expensive qualified NDT personnel.

Acknowledgements

This research was been supported by the project TRIO č. FV10757 "Thermovision system for non-destructive testing of weld joints", financed by MPO ČR and SGS16/217/OHK2/3T/12.

References

[1] L. Kolařík, J. Sova, M. Kolaříková, L. Forejtová. Termovizní kontrola svarových spojů. *MM Průmyslové spektrum* **3**:2–3, 2017.

[2] Óscar Martín, P. D. Tiedra, M. López, et al. Quality prediction of resistance spot welding joints of 304 austenitic stainless steel. *Materials & Design* **30**(1):68 – 77, 2009. DOI:10.1016/j.matdes.2008.04.050.

[3] M. Dvorak, T. Pilvousek. *Materials used for bodywork, Company documents*. ŠKODA Auto a.s., 2014.

[4] H.-T. Lee, M. Wang, R. Maev, E. Maeva. A study on using scanning acoustic microscopy and neural network techniques to evaluate the quality of resistance spot welding. *The International Journal of Advanced Manufacturing Technology* **22**:727–732, 2003. DOI:10.1007/s00170-003-1599-9.

[5] ISO14373:2015 - Resistance welding - Procedure for spot welding of uncoated and coated low carbon steels. Standard, International Organization for Standardization, 2015.

[6] M. Pouranvari, A. Abedi, P. Marashi, M. Goodarzi. Effect of expulsion on peak load and energy absorption of low carbon resitance spot welds. *Science and Technology of Welding & Joining* **13**:39–43, 2008. DOI:10.1179/174329307X249342.

[7] J. Matoušek. UT kontrola odporových bodových svarů. Tech. rep., ATG, 2008.

[8] Ó. Martín, M. Pereda, J. Ignacio Santos, J. M. Galán. Assessment of resistance spot welding quality based on ultrasonic testing and tree-based techniques. *Journal of Materials Processing Technology* **214**:2478–2487, 2014. DOI:10.1016/j.jmatprotec.2014.05.021.

[9] T. Y. Afek, M. Bron. Improving SpotWeld inspection results using Phased-Array (PA) capabilities, Scanmaster Systems Ltd. `www.ndt.net/article/ecndt2018/papers/ecndt-0122-2018.pdf`, 2018. Accessed: 10 November 2018.

[10] H. T. Lee, R. Maev, E. Y. Maeva, S. A. Titov. Method and system for assessing quality of spot welds, 2009. US Government Patent No. US7516022B2.

[11] S. Lee, J. Nam, W. Hwang, et al. A study on integrity assessment of the resistance spot weld by infrared thermography. *Procedia Engineering* **10**:1748–1753, 2011. DOI:10.1016/j.proeng.2011.04.291.

[12] J. Schlichting, S. Brauser, L.-A. Pepke, et al. Thermographic testing of spot welds. *NDT & E International* **48**:23–29, 2012. DOI:10.1016/j.ndteint.2012.02.003.

[13] A. Runnemalm, J. Ahlberg, A. Appelgren, S. Sjökvist. Automatic inspection of spot welds by thermography. *Journal of Nondestructive Evaluation* **33**:398–406, 2014. DOI:10.1007/s10921-014-0233-0.

[14] A. . C. Traub. Control of spot weld quality by infrared thermal sensing, 1980. US Government Patent No. US4214164A.

[15] D. W. Hahn, M. N. Özisik (eds.). *Heat conduction*. Wiley, 3rd edn., Wiley.

[16] P. Landecká. *A way of ensuring quality in the process of bodywork welding*. Bachelor's thesis, ŠKODA AUTO University, Czech Republic, 2011. In Czech.

[17] R. P. Madding. Emissivity measurement and temperature correction accuracy considerations. In *SPIE Conference on Thermosense XXI*, vol. 3700. Florida, 1999. DOI:10.1117/12.342307.

[18] X. P. Maldague, P. O. Moore (eds.). *Nondestructive Testing Handbook, Third Edition: Volume 3, Infrared and Thermal Testing (IR)*. ASNT, 2001.

[19] P. Litos. *Emissivity and Temperature Field Measurements in Physical Technologies*. Ph.D. thesis, University of West Bohemia, Czech Republic, 2006. In Czech.

[20] M. Kolaříková, L. Kolařík, L. Forejtová, et al. The effect of parameters at resistence spot welding on quality of spot joint of steel DC06. *Metal* 2018.

[21] J. Svoboda. Thermodiagnostics. Technical manual.

[22] P. Mach. *Evaluation of the quality of resistance spot welded joints by thermography*. Bachelor's thesis, Faculty of Mechanical Engineering, Czech Technical University in Prague, Czech Republic, 2017. In Czech.

[23] Š. Holub. *NDT inspection of resistance spot welds*. Bachelor's thesis, Faculty of Mechanical Engineering, Czech Technical University in Prague, Czech Republic, 2017. In Czech.